

Recollision of excited electron in below-threshold nonsequential double ionization

Xiaolei Hao,¹ Yuxing Bai¹, Chan Li¹, Jingyu Zhang¹, Weidong Li¹, Weifeng Yang^{2,*}, MingQing Liu³, and Jing Chen^{3,4†}

¹*Institute of Theoretical Physics and Department of Physics,*

State Key Laboratory of Quantum Optics and Quantum Optics Devices,

Collaborative Innovation Center of Extreme Optics, Shanxi University, Taiyuan 030006, China

²*Department of Physics, College of Science, Shantou University, Shantou, Guangdong 515063, China*

³*Institute of Applied Physics and Computational Mathematics, P. O. Box 8009, Beijing 100088, China and*

⁴*Shenzhen Key Laboratory of Ultraintense Laser and Advanced Material Technology,*

Center for Advanced Material Diagnostic Technology, and College of Engineering Physics,

Shenzhen Technology University, Shenzhen 518118, China

(Dated: June 14, 2021)

Consensus has been reached that recollision, as the most important post-tunneling process, is responsible for nonsequential double ionization process in intense infrared laser field, however, its effect has been restricted to interaction between the first ionized electron and the residual univalent ion so far. Here we identify the key role of recollision between the second ionized electron and the divalent ion in the below-threshold nonsequential double ionization process by introducing a Coulomb-corrected quantum-trajectories method, which enables us to well reproduce the experimentally observed cross-shaped and anti-correlated patterns in correlated two-electron momentum distributions, and also the transition between these two patterns. Being significantly enhanced relatively by the recapture process, recolliding trajectories of the second electron excited by the first- or third-return recolliding trajectories of the first electron produce the cross-shaped or anti-correlated distributions, respectively. And the transition is induced by the increasing contribution of the third return with increasing pulse duration. Our work provides new insight into atomic ionization dynamics and paves the new way to imaging of ultrafast dynamics of atoms and molecules in intense laser field.

PACS numbers: 133.80.Rv, 33.80.Wz, 42.50.Hz

Recollision is responsible for many intriguing strong-field phenomena, such as high-order above-threshold ionization (HATI), high harmonics generation (HHG), and nonsequential double ionization (NSDI), and also serves as the foundation of attosecond physics (see, e.g., Refs. [1–4] for reviews and references therein). In the recollision picture [5, 6], an electron is liberated from the neutral atom or molecule through tunneling, then is driven back by the laser field to collide with the parent ion elastically or inelastically, or recombine with the ion, resulting in HATI, NSDI and HHG, respectively. Since the electron strongly interacts with the ion, the products upon recollision carry information of the parent ion, and can be used to probe its structure and dynamics. Based on the recollision process, different methods, such as laser-induced electron diffraction (LIED) [7] and laser-induced electron inelastic diffraction (LIID) [8], are proposed and successfully applied in imaging of atomic and molecular ultrafast dynamics and structure with unprecedented spatial-temporal resolution [8–15]. However, the recollision in the above-mentioned strong-field processes and ultrafast imaging methods is limited to interaction between the ionized electron and univalent ion.

In the NSDI process, one electron (e_1) firstly experi-

ences a recollision with the parent univalent ion and deliver energy to the bounded electron (e_2). In the below-threshold regime, the maximal kinetic energy of e_1 upon recollision is smaller than the ionization potential of e_2 , so e_2 can be only pumped to an excited state, as illustrated in Fig. 1. Then e_2 is ionized from the excited state by the laser field at a later time, dubbed as recollision excitation with subsequent ionization (RESI) process. Usually, it is believed that e_2 will travel directly to the detector [16–19]. However, after tunneling ionization, e_2 may be driven back to recollide with the divalent ion or be recaptured into a Rydberg state of ion as illustrated in Fig. 1. Due to the strong Coulomb field of the divalent ion, these post-tunneling dynamics may be prominent. It has been recently reported experimentally and theoretically that the probability of recapture in double ionization, dubbed as frustrated double ionization (FDI), is much higher than expectation [20, 21].

In this work, by introducing a Coulomb-corrected quantum-trajectories (CCQT) method, we identify the key role played by the recollision between the second ionized electron and the divalent ion in the below-threshold NSDI process. We find that, only when this recollision is included, the experimentally observed cross-shaped [22, 23] and anti-correlated [24] patterns of correlated electron momentum distribution (CEMD), and also the transition between them [25], can be well reproduced.

To describe the below-threshold NSDI process both coherently and quantitatively, it has to incorporate both

*Electronic address: wfyang@stu.edu.cn

†Electronic address: chenjing@iapcm.ac.cn

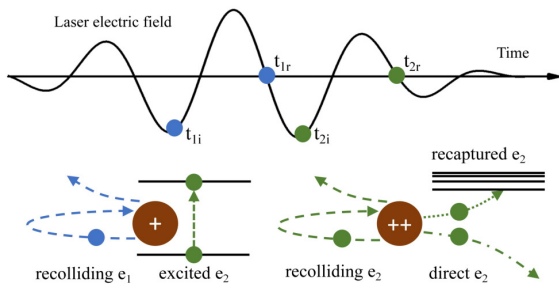


FIG. 1: Sketch map to illustrate the below-threshold NSDI process. At time t_{1i} , e_1 is first ionized by the laser field, then it is driven back to collide the parent univalent ion and excites e_2 at time t_{1r} . e_2 is ionized from the excited state by the laser field at a later time t_{2i} . After that, e_2 may travel directly to the detector, or it may be driven back to recollide with the divalent ion similar to e_1 , or it may also be recaptured into a Rydberg state of ion.

the quantum effect and the Coulomb interaction between the residual ion and the ionized electrons in a uniform theory. To achieve this, we introduce a Coulomb-corrected quantum-trajectories (CCQT) method by taking advantage of the well-developed Coulomb-corrected methods dealing with single-electron dynamics. The transition magnitude is expressed as (atomic units $m = \hbar = e = 1$ are used)

$$M(\tilde{\mathbf{p}}_1, \tilde{\mathbf{p}}_2) = \sum_s M_{\tilde{\mathbf{p}}_2}^{(3)}(t_{2i}^s, t_{1r}^s) M_{\tilde{\mathbf{p}}_1}^{(2)}(t_{1r}^s) M_{\tilde{\mathbf{p}}_1}^{(1)}(t_{1r}^s, t_{1i}^s), \quad (1)$$

in which different trajectories labelled with s are summed coherently. $M_{\tilde{\mathbf{p}}_1}^{(1)}(t_{1r}^s, t_{1i}^s)$, describing the tunneling ionization of e_1 at t_{1i}^s and its subsequent propagation in the laser field until colliding with the parent ion at time t_{1r}^s , is calculated using the quantum-trajectory Monte Carlo (QTMC) method [26, 27] which is efficient to obtain large amount of hard-collision trajectories. Trajectories with minimum distance from the ion less than 1 a.u. are selected to consider the hard collision for the subsequent calculation. Upon collision, e_1 will excite e_2 and then move to the detector. This excitation process is described by $M_{\tilde{\mathbf{p}}_1}^{(2)}(t_{1r}^s)$ which is calculated with conventional S-matrix theory. Finally, e_2 is ionized through tunneling at t_{2i}^s from the excited state, and then propagates in the laser field until the end of the pulse, which is described by $M_{\tilde{\mathbf{p}}_2}^{(3)}(t_{2i}^s, t_{1r}^s)$ calculated with the Coulomb-corrected strong field approximation (CCSFA) method [28]. The sin-squared pulse shape is employed in our calculation. A model potential [29] is applied to mimic the Coulomb field of Ar^{2+} felt by e_2 in its propagation. Only the first excited state $3s3p^6$ with zero magnetic quantum number [30] is included in the present calculations. The depletion of the excited state is also taken into account in calcu-

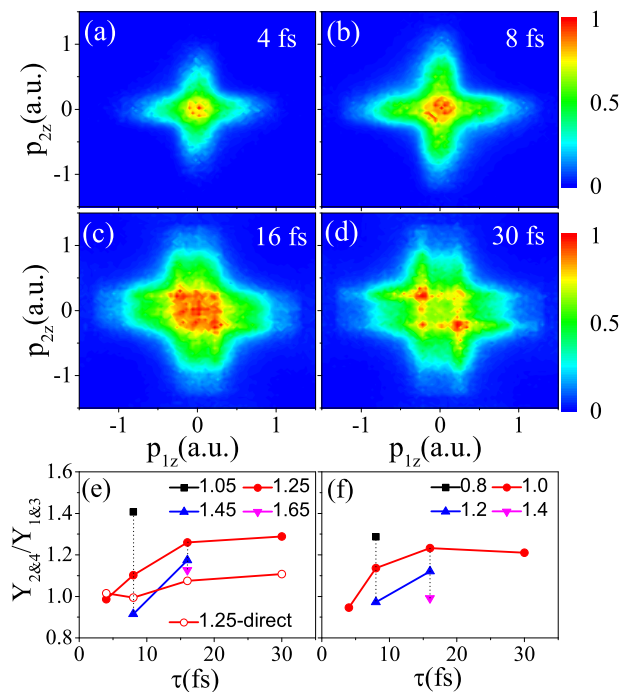


FIG. 2: (a)-(d) Simulated CEMDs of Ar for different laser pulse durations at the intensity of 1.25×10^{14} W/cm². The CEPs are averaged. Each CEMD is normalized to itself. (e) Simulated yield ratio $Y_{2\&4}/Y_{1\&3}$ for different pulse durations and different intensities. $Y_{1\&3}$ ($Y_{2\&4}$) denotes the integrated yield in the first and third (the second and fourth) quadrants in the CEMD. The numbers given in the legends denote peak laser intensities with units of 10^{14} W/cm². The open circles are calculated by only considering direct trajectories of e_2 (see text for details). (f) Measured results extracted from Ref.[25]. The black short-dashed lines in (e) and (f) serve as indications of the intensity dependence.

lating $M_{\tilde{\mathbf{p}}_2}^{(3)}(t_s, t'_s)$ [18] (see the method in Supplement 1).

Fig. 2 displays the calculated results for Ar under different pulse durations to compare with the experimental results in Ref. [25]. Intensities higher than the measured ones by 0.25×10^{14} W/cm² are used in the present calculations (see Supplement 1 for details of the fitting procedure). As shown in Fig. 2, for shorter pulse durations (4 fs and 8 fs), the distributions show a cross shape with the maxima lying at the origin. While for longer pulses (16 fs and 30 fs), the electrons are more homogeneously distributed over the four quadrants, actually, prefer the second and fourth quadrants, which indicates an anti-correlation. This transition of CEMD from cross-shaped to anti-correlated patterns is in agreement with the measured results reported in Ref. [25], although there is some discrepancy in details. In the measurement, the transition occurs when pulse duration increases from 4 fs to 8 fs, whereas in Fig. 2 it occurs when pulse duration increases from 8 fs to 16 fs. This discrepancy may be due to that the pulse shape and duration employed in our calculations are not exactly the same as that in the

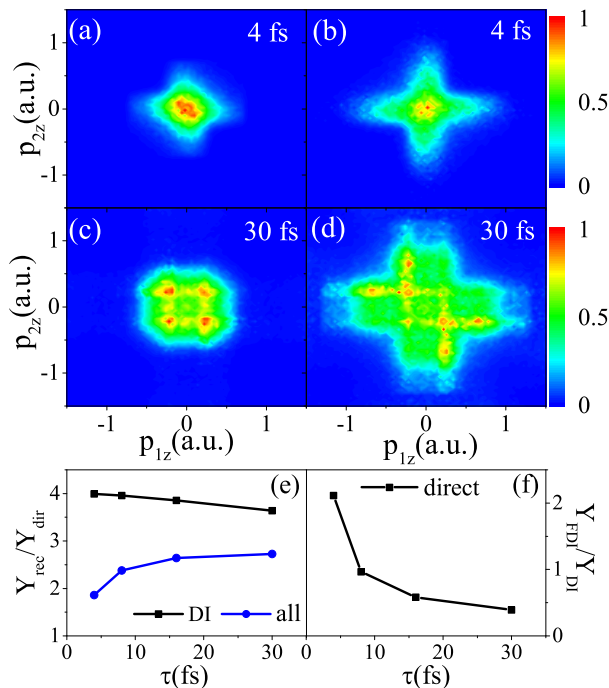


FIG. 3: CEMDs corresponding to direct trajectories [(a) and (c)] and recolliding trajectories [(b) and (d)] of e_2 . Each CEMD is normalized to itself. (e) Pulse-duration dependence of Y_{rec}/Y_{dir} , the ratio between the integrated yields of recolliding and direct trajectories for e_2 for all events or only double ionization (DI) events. (f) Pulse-duration dependence of Y_{FDI}/Y_{DI} , the ratio between the probabilities of FDI and DI when e_2 is confined to direct trajectories. The laser intensity is 1.25×10^{14} W/cm 2 .

measurements.

To quantitatively characterize the CEMD, in Fig. 2(e) we plot the ratio $Y_{2\&4}/Y_{1\&3}$ for different pulse durations and different intensities. $Y_{1\&3}$ ($Y_{2\&4}$) denotes the integrated yield in the first and third (the second and fourth) quadrants. We also present the measured results [25] in Fig. 2(f) for comparison. In general, the simulation reproduces most of the features in the measured results. The ratio increases with pulse duration and becomes saturated at 16 fs when the intensity is fixed, and it decreases with laser intensity both for pulse durations of 8 fs and 16 fs. However, compared with the measured results, the simulation obviously overestimates the ratio for the highest intensity. This discrepancy can be attributed to that the contribution of the process that e_2 is directly knocked out by e_1 , whose distribution mainly locates in the first and third quadrants, becomes more significant with increasing intensity, but is not included here.

In Fig. 3, we present CEMDs corresponding to recolliding trajectories and direct trajectories of e_2 at 4 fs and 30 fs, respectively. Here, we define it as the recolliding trajectory if the minimal distance of e_2 from the residual ion is less than the tunnel exit. Otherwise, it is the direct trajectory. Since momenta of direct trajectories of e_2 are much smaller than that of recolliding trajectories,

CEMDs for direct trajectories are localized around the origin for both 4 fs and 30 fs pulses, as shown in Figs. 3(a) and 3(c). Whereas the CEMD for recolliding trajectories exhibits a cross structure at 4 fs [Fig. 3(b)], and exhibits an anti-correlated pattern at 30 fs [Fig. 3(d)]. Meanwhile, recolliding trajectories of e_2 have dominant contributions for all pulse durations as depicted by the ratio Y_{rec}/Y_{dir} (Y_{rec} and Y_{dir} denote the yields of recolliding and direct trajectories, respectively) for double ionization (DI) events in Fig. 3(e), as a consequence, the total CEMDs also shows a cross or an anti-correlated pattern at 4 fs or 30 fs, respectively.

But why the relative contribution of the recolliding trajectories of e_2 is so high? Intuitively, the Coulomb focusing effect imposed on e_2 by the divalent cation, which is much stronger than that of the univalent cation in ATI process, will effectively enhance the probability of recollision. We can indeed see this clearly from Fig. 3(e) in which the ratio Y_{rec}/Y_{dir} with all events included is greater than 1. But it is still much smaller than the ratio considering only DI events. This deviation is the result of the important contribution of recapture or FDI process. More than two-thirds of direct e_2 are recaptured into the Rydberg states of Ar^+ at 4fs, and the probability of FDI for direct e_2 decreases quickly with increasing pulse duration, as shown in Fig. 3(f). Compared with recolliding trajectory of e_2 , direct e_2 cannot move far away from Ar^{2+} at the end of the pulse due to its much lower momentum, especially in shorter laser pulse, therefore is easier to be recaptured by the strong Coulomb field of the divalent ion. More direct e_2 being recaptured means fewer of them contribute to DI, resulting in larger relative contribution of recolliding trajectories of e_2 to DI. In brief, the enhanced FDI probability significantly enlarges the relative contribution of recolliding trajectories of e_2 to DI, and eventually induces the experimentally observed cross-shaped and anti-correlated patterns. In addition, this point is strongly supported by the fact that when only the direct trajectories of e_2 are considered, the calculated $Y_{2\&4}/Y_{1\&3}$ is significantly different from the experimental result [see Fig. 2(e)].

The specific pattern of CEMD also requires the appropriate momentum of e_1 which is determined by the microscopic dynamics of the recollision process for e_1 . In the recollision process of e_1 , it may miss the parent ion at its first return but collide with the ion at the subsequent returns. In our model, the different-return trajectories of e_1 can be distinguished according to the travel time t_t defined as the interval between the ionization time t_{1i} and the recollision time t_{1r} . For trajectories with t_t in the interval $[(n/2)T, ((n+1)/2)T]$ (T is the optical cycle), we denote them as the n th-return trajectories [31, 32]. According to our calculations, the first- and third-return recolliding trajectories of e_1 are dominant for the laser parameters interested here. For other returns, either the return energy is too small to excite e_2 , or the collision probability is negligible due to the spreading of the wave packet. In Figs. 4(a) and 4(b), we present the CEMDs

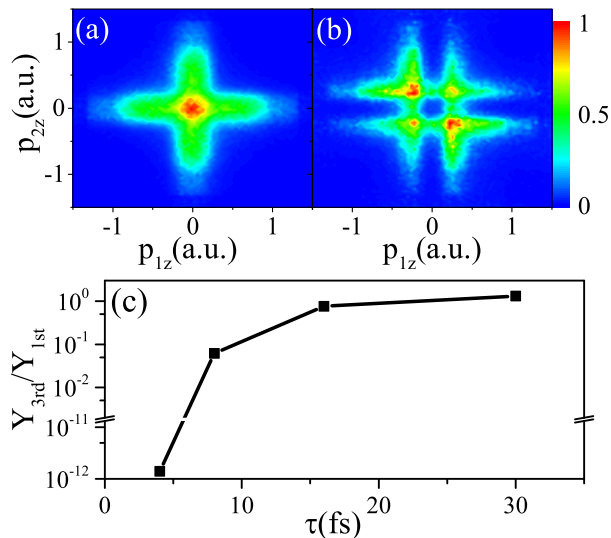


FIG. 4: CEMDs in 30 fs, 1.25×10^{14} W/cm² laser pulse when the trajectories of e_1 are confined to the first return (a) or the third return (b). Each CEMD is normalized to itself. (c) Pulse-duration dependence of Y_{3rd}/Y_{1st} , the ratio of the integrated yield of the third-return to that of the first-return trajectories of e_1 .

corresponding to the first- and third-return trajectories of e_1 , respectively, in 1.25×10^{14} W/cm², 30 fs laser pulse. Note that all trajectories of e_2 (direct and recolliding trajectories) are included. The CEMD for the first-return trajectories of e_1 [Fig. 4(a)] shows a cross-shaped pattern, whereas that for the third-return trajectories [Fig. 4(b)] exhibits an anti-correlated pattern. As shown in Fig. 4(c), the ratio of the integrated yield of the third-return trajectories to that of the first-return increases quickly with increasing pulse duration. Correspondingly, the CEMD changes from a cross-shaped to an anti-correlated pattern. Therefore, the transition between the two patterns of CEMD with increasing pulse duration is the result of increasing contribution of the third-return trajectories of e_1 . The significant contribution of the third-return trajectories can be attributed to the Coulomb focusing effect from the univalent cation. The similar effect has also been reported for high-order ATI process [32].

Next, we will explain how the cross-shaped and anti-correlated patterns of CEMDs are formed by the recolliding trajectories of the two electrons. Without indistinguishability symmetrization, the first-return trajectories of e_1 will show a band-like distribution along the $p_{1z} = 0$ axis with the maxima away from the origin, i. e., vanishing momentum of e_1 but much higher momentum of e_2 [Fig. 5(b)]. Whereas the CEMD for the third-return consists of two bands and the maximum of the left (right) band lies in the up (low) part, giving rise to an anti-correlation [Fig. 5(c)]. These band-like distributions can be understood as follows. The final momentum of

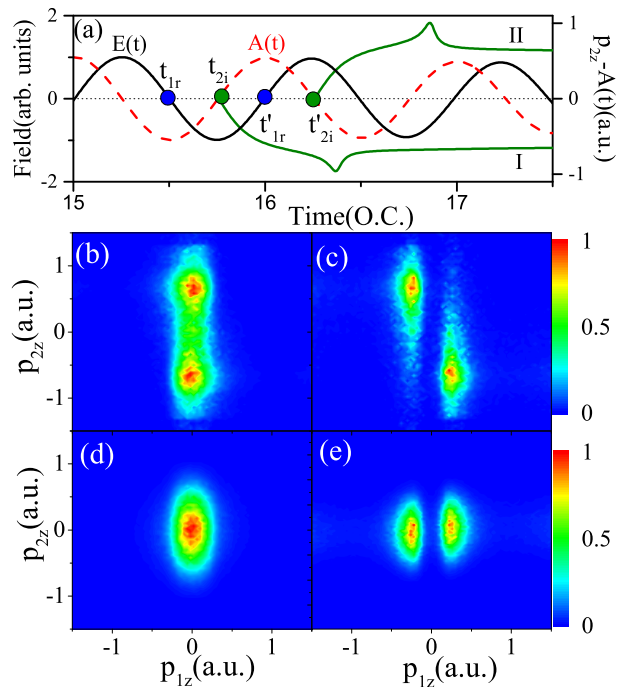


FIG. 5: (a) Schematic representation of the laser electric field $\mathbf{E}(t)$ and the corresponding vector potential $\mathbf{A}(t)$ for pulse duration of 30 fs. e_1 collides with the ion most probably at the crossing of $\mathbf{E}(t)$ at t_{1r} or t'_{1r} . Upon the collision, e_2 is excited, and then is ionized most probably at the peak of the laser field at t_{2i} or t'_{2i} . The subsequent evolution of the canonical momentum $p_{2z} - A(t)$ for the recolliding trajectories of e_2 , denoted as I and II, are presented to illustrate the Coulomb-field effect of Ar^{2+} . (b) and (c) CEMDs without performing electron indistinguishability symmetrization, and only recolliding trajectories of e_2 with ionization time nearest the collision time of e_1 are included. (d) and (e) CEMDs calculated by replacing the ionization amplitude $M_{\mathbf{p}_2}^{(3)}$ in Eq. (1) with the standard SFA. Trajectories of e_1 are confined to the first return in (b) and (d), and the third return in (c) and (e). Each CEMD is normalized to itself.

e_1 is determined by the residual momentum after exciting e_2 and the drift momentum it obtains from the laser field. Since forward scattering is favored in this inelastic scattering process, the residual momentum and the drift momentum are in opposite directions and will cancel with each other. At the present intensity (1.25×10^{14} W/cm²), the magnitudes of them for the first-return trajectories of e_1 are nearly equal, resulting in a vanishing momentum of e_1 . When the laser intensity increases, the band will become tilted towards the main diagonal [23] due to the faster-increasing residual momentum. For the third-return, its return energy is smaller than that of the first-return, so the residual momentum is not enough to compensate the drift momentum, resulting in a non-vanishing momentum of e_1 . Since electrons ionized at times separated by a half optical cycle will have opposite momenta, there is one band on each side of $p_{1z} = 0$ axis.

Actually, there are also two bands for the first return, but they merge together.

The anti-correlation between the two electrons for the third-return trajectories of e_1 is illustrated in Fig. 5(a). The recollision of e_1 most probably occurs around the crossing of the electric field at t_{1r} or t'_{1r} . Since the magnitude of the drift momentum after recollision, which is equal to $-\mathbf{A}(t_r)$ (vector potential at the recollision time), is larger than the residual momentum for the third-return recolliding trajectories of e_1 , its final momentum is in the direction of the drift momentum. If the recollision of e_1 occurs at t_{1r} , the final momentum of e_1 will be positive, corresponding to the right band in Fig. 5(c). Upon recollision, e_2 is pumped to the first excited state, then it is most probably ionized at the subsequent electric field peak at t_{2i} . If the Coulomb attraction of the ion is not considered and no recollision occurs, e_2 will have vanishing final momentum. This can be seen clearly in Figs. 5(d) and 5(e), in which the CEMDs are obtained by calculating $M_{\mathbf{p}_2}^{(3)}$ in Eq. (1) with the standard SFA. But if the ionic Coulomb potential is taken into account, momenta of e_2 for recolliding trajectories (trajectory I) shift to the negative direction, opposite to the direction of the final momentum of e_1 [see Fig. 5(a)]. This is exactly the situation of the right-band distribution in Fig. 5(c). The left band corresponds to the situation that e_1 recollides with the ion at t'_{1r} and e_2 is ionized at t'_{2i} . As a consequence, the two electrons are emitted back-to back

and the CEMD exhibits an anti-correlated pattern. In addition, it is also possible that the recollision of e_1 occurs at t_{1r} while e_2 is ionized at t'_{2i} , which will produce a correlated CEMD. But since its contribution is smaller due to the depletion effect of the excited state, the total CEMD will still exhibit an anti-correlated pattern.

In conclusion, we propose a Coulomb-corrected quantum-trajectories (CCQT) method to describe the below-threshold NSDI process both coherently and quantitatively. It enables us to well reproduce different kinds of CEMDs observed in experiments, and uncover the rich underlying physics which is enhanced by the Coulomb field of univalent and divalent ions, including the multi-return trajectories of the first ionized electron e_1 , the recollision and recapture processes of the second ionized electron e_2 . Especially, recollision process of e_2 , which is enhanced relatively by the recapture process of e_2 , is found to play an important role in electron-electron correlation. We expect that the recollision process of e_2 can be applied to develop a new scheme to image the ultrafast evolution of the molecular structure and dynamics induced by the strong laser field.

This work was partially supported by the National Key Program for S&T Research and Development (No. 2019YFA0307700 and No. 2016YFA0401100), the National Natural Science Foundation of China (Grants No. 11874246, No. 91950101, No. 11774215).

-
- [1] M. Protopapas, C. H. Keitel and P.L. Knight, Atomic physics with super-high intensity lasers, *Rep. Prog. Phys.* **60**, 389 (1997).
- [2] W. Becker, F. Grasbon, R. Kopold, D. B. Milošević, G. G. Paulus, and H. Walther, Above-threshold ionization: form classical features to quantum effects, *Adv. At. Mol. Opt. Phys.* **48**, 35 (2002).
- [3] W. Becker, X. J. Liu, P. J. Ho, and J. H. Eberly, Theories of photoelectron correlation in laser-driven multiple atomic ionization, *Rev. Mod. Phys.* **84**, 1011 (2012).
- [4] F. Krausz and M. Ivanov, Attosecond physics, *Rev. Mod. Phys.* **81**, 163 (2009).
- [5] P. B. Corkum, Plasma perspective on strong-field multiphoton ionization, *Phys. Rev. Lett.* **71**, 1994 (1993).
- [6] K. J. Schafer, Baorui Yang, L. F. DiMauro, and K. C. Kulander, Above threshold ionization beyond the high harmonic cutoff, *Phys. Rev. Lett.* **70**, 1599 (1993).
- [7] T. Morishita, A.-T. Le, Z. Chen, and C. D. Lin, Accurate retrieval of structural information from laser-induced photoelectron and high-order harmonic spectra by few-cycle laser pulses, *Phys. Rev. Lett.* **100**, 013903 (2008).
- [8] W. Quan, X. L. Hao, X. Q. Hu, R. P. Sun, Y. L. Wang, Y. J. Chen, S. G. Yu, S. P. Xu, Z. L. Xiao, X. Y. Lai, X. Y. Li, W. Becker, Y. Wu, J. G. Wang, X. J. Liu and J. Chen, Laser-induced inelastic diffraction from strong-field double ionization. *Phys. Rev. Lett.* **119**, 243203 (2017).
- [9] M. Okunishi, T. Morishita, G. Prümper, K. Shimada, C. D. Lin, S. Watanabe, and K. Ueda, Experimental retrieval of target structure information from laser-induced rescattered photoelectron momentum distributions, *Phys. Rev. Lett.* **100**, 143001 (2008).
- [10] D. Ray, B. Ulrich, I. Bocharova, C. Maharjan, P. Ranitovic, B. Gramkow, M. Magrakvelidze, S. De, I. V. Litvinyuk, A. T. Le, T. Morishita, C. D. Lin, G. G. Paulus, and C. L. Cocke, Large-angle electron diffraction structure in laser-induced rescattering from rare gases, *Phys. Rev. Lett.* **100**, 143002 (2008).
- [11] M. Meckel, D. Comtois, D. Zeidler, A. Staudte, D. Pavičić, H. C. Bandulet, H. Pépin, J. C. Kieffer, R. Dörner, D. M. Villeneuve and P. B. Corkum, Laser-induced electron tunneling and diffraction, *Science* **320**, 1478 (2008).
- [12] C. I. Blaga, J. Xu, A. D. DiChiara, E. Sistrunk, K. Zhang, P. Agostini, T. A. Miller, L. F. DiMauro and C. D. Lin, Imaging ultrafast molecular dynamics with laser-induced electron diffraction, *Nature* **483**, 194 (2012).
- [13] H. Niikura, F. Légaré, R. Hasbani, A. D. Bandrauk, M. Y. Ivanov, D. M. Villeneuve and P. B. Corkum, Controlling electron-ion-recollision dynamics with attosecond precision, *Nature* **417**, 917 (2002).
- [14] J. Itatani, J. Levesque, D. Zeidler, H. Niikura, H. Pépin, J. C. Kieffer, P. B. Corkum and D. M. Villeneuve, Tomographic imaging of molecular orbitals, *Nature* **432**, 867 (2004).
- [15] B. Wolter, M. G. Pullen, A.-T. Le, M. Baudisch, K. Doblhoff-Dier, A. Senftleben, M. Hemmer, C. D. Schröter, J. Ullrich, T. Pfeifer, R. Moshhammer, S. Gräfe,

- O. Vendrell, C. D. Lin, and J. Biegert, Ultrafast, electron diffraction imaging of bond breaking in di-ionized acetylene, *Science* **354**, 308 (2016).
- [16] T. Shaaran, M. T. Nygren, and C. Figueira de Morisson Faria, Laser-induced nonsequential double ionization at and above the recollision-excitation-tunneling threshold, *Phys. Rev. A* **81**, 063413 (2010).
- [17] B. Wang, Y. Guo, J. Chen, Z. Yan, and P. Fu, Frequency-domain theory of nonsequential double ionization in intense laser fields based on nonperturbative QED, *Phys. Rev. A* **85**, 023402 (2012).
- [18] X. L. Hao, J. Chen, W. D. Li, B. Wang, X. Wang, and W. Becker, Quantum effects in double ionization of Argon below the threshold intensity, *Phys. Rev. Lett.* **112**, 073002 (2014).
- [19] A. S. Maxwell, and C. Figueira de Morisson Faria, Controlling below-threshold nonsequential double ionization via quantum interference, *Phys. Rev. Lett.* **116**, 143001 (2016).
- [20] S. Larimian, S. Erattupuzha, A. Baltuška, M. Kitzler-Zeiler, and X. Xie, Frustrated double ionization of argon atoms in strong laser fields, *Phys. Rev. Research* **2**, 013021 (2020).
- [21] S. Chen, J. Chen, G. G. Paulus, and H. Kang, Strong-field frustrated double ionization of argon atoms, *Phys. Rev. A* **102**, 023103 (2020).
- [22] B. Bergues, M. Kübel, N. Johnson, B. Fischer, N. Camus, K. Betsch, O. Herrwerth, A. Senfleben, A. Saylor, T. Rathje, T. Pfeifer, I. Ben-Itzhak, R. Jones, G. Paulus, F. Krausz, R. Moshhammer, J. Ullrich, and M. Kling, Attosecond tracing of correlated electron-emission in non-sequential double ionization, *Nat. Commun.* **3**, 813 (2012).
- [23] M. Kübel, C. Burger, N. G. Kling, T. Pischke, L. Beaufore, I. Ben-Itzhak, G. G. Paulus, J. Ullrich, T. Pfeifer, R. Moshhammer, M. F. Kling, and B. Bergues, Complete characterization of single-cycle double ionization of argon from the nonsequential to the sequential ionization regime, *Phys. Rev. A* **93**, 053422 (2016).
- [24] Y. Liu, S. Tschuch, A. Rudenko, M. Dürr, M. Siegel, U. Morgner, R. Moshhammer, and J. Ullrich, Strong-field double ionization of Ar below the recollision threshold, *Phys. Rev. Lett.* **101**, 053001 (2008).
- [25] M. Kübel, K. J. Betsch, N. G. Kling, A. S. Alnaser, J. Schmidt, U. Kleineberg, Y. Deng, I. Ben-Itzhak, G. G. Paulus, T. Pfeifer, J. Ullrich, R. Moshhammer, M. F. Kling and B. Bergues, Non-sequential double ionization of Ar: from the single- to the many-cycle regime, *New J. Phys.* **16**, 033008 (2014).
- [26] M. Li, J. Geng, H. Liu, Y. Deng, C. Wu, L. Peng, Q. Gong, and Y. Liu, Classical-quantum correspondence for above-threshold ionization, *Phys. Rev. Lett.* **112**, 113002 (2014).
- [27] X. Song, C. Lin, Z. Sheng, P. Liu, Z. Chen, W. Yang, S. Hu, C. D. Lin, and J. Chen, Unraveling nonadiabatic ionization and Coulomb potential effect in strong-field photoelectron holography, *Sci. Rep.* **6**, 28392 (2016).
- [28] T. M. Yan, S. V. Popruzhenko, M. J. J. Vrakking and D. Bauer, Low-energy structures in strong field ionization revealed by quantum orbits, *Phys. Rev. Lett.* **105**, 253002 (2010).
- [29] X. Tong and C. Lin, Empirical formula for static field ionization rates of atoms and molecules by lasers in the barrier-suppression regime, *J. Phys. B* **38**, 2593 (2005).
- [30] K. G. Dyall, I. P. Grant, F. A. Parpia, and E. P. Plummer, GRASP: A general-purpose relativistic atomic structure program, *Comput. Phys. Commun.* **55**, 425 (1989).
- [31] X. L. Hao, W. D. Li, J. Liu and J. Chen, Effect of the electron initial longitudinal velocity on the nonsequential double-ionization process, *Phys. Rev. A* **83**, 053422 (2011).
- [32] X. L. Hao, Y. X. Bai, X. Y. Zhao, C. Li, J. Y. Zhang, J. L. Wang, W. D. Li, C. L. Wang, W. Quan, X. J. Liu, Z. Shu, M. Liu, and J. Chen, Effect of Coulomb field on laser-induced ultrafast imaging methods, *Phys. Rev. A* **101**, 051401(R)(2020).